Angewandte Chemie
Eine Zeitschrift der Gesellschaft Deutscher Chemiker

Supporting Information

The Metallocene Battery: Ultrafast Electron Transfer Self Exchange Rate Accompanied by a Harmonic Height Breathing

Seyyed Mohsen Beladi-Mousavi, Shamaila Sadaf, Ann-Kristin Hennecke, Jonas Klein, Arsalan Mado Mahmood, Christian Rüttiger, Markus Gallei, Fangyu Fu, Eric Fouquet, Jaime Ruiz, Didier Astruc, and Lorenz Walder**

anie_202100174_sm_miscellaneous_information.pdf

Table of content

1- Experimental section

Materials. All the chemicals and solvents were from Sigma–Aldrich and used as received without further purification unless otherwise stated. Solvents for electrochemistry and spectroscopy were of 99.9% purity. Graphene oxide (GO) was from *"Graphenea"* delivered as an aqueous solution (4 mg GO in 1 ml H_2O). PFc with the following procedures/characteristics was used and prepared: size exclusion chromatography (SEC) (conventional vs PS standards), PDI: 1.26, Mw: 11640 g mol^{-1}, as earlier reported.[1] PCo with the following procedures/characteristics was used and prepared: SEC, PDI: 1.24, Mw: 4938 g mol^{-1}, as earlier reported.[2]

Preparation of PCo@GO. a) 5/1 weight ratio: 5.8 mg PCo (dissolved in 0.5 ml DMF and 2.5 ml H_2O) was dropwise added to 0.29 ml GO solution (4 mg in 1 ml H_2O) under sonication in an ultrasonic water bath for 10 min. b) Zeta potential measurements: Appropriate volumes of the PCo solution (2mg in 1ml H_2O) were added under sonication over 15 min to 0.5 ml of the GO solution (1mg GO in 20 ml H_2O), and the final mixtures were diluted to 5 ml volume under sonication for another 5 min.

Preparation of PFc@GO. The solution was prepared as described using a PFc^{x+}/GO^{m-} weight ratio of 5:1.[2]

Electrode preparation. a) up to 8 µm thick films: drop casting of polymer@GO solution (each drop: 5-10 µl) on the current collector followed by drying at 60°C for 10 min. b) electrodes for STM: The HOPG electrode was dipped into a solution of Polymer@GO (3/1, 4×10^{-9} mol subunits cm^{-2}) for 1 minute, then the excess solution was gently sucked off with a tissue paper.

Electrochemical measurements. The electrochemical measurements were performed in surface confined state on a glassy carbon (GC) electrode (0.071 cm^2, Metrohm, 6.0804.010), or on a 0.5 inch quartz crystal resonators (0.28 cm^2 gold electrodes, KVG Quartz Crystal Technology GmbH), or on HOPG (5*5 mm piece from Schaefer Technology GmbH), or on flexible graphite foil (SGL

GROUP, SIGRACET Bipolar plate TF6: 0.2 mm thick), or on graphite electrode (SGL GROUP, SIGRACELL PV15 graphite plate, 0.7 mm thick). The electrochemical GO/rGO transformation was performed by consecutive CV scans (between -0.4 and -1.2 V vs. Ag/AgCl) at 5-50 mV s^{-1} until the electrocatalytic reduction current disappeared. CVs were measured using an Autolab potentiostat (PGSTAT 20) interfaced to a computer with the GPS software (version 4.9).

Electrochemical Quartz Crystal Microbalance (ec-QCM). The *ec*-QCM experiments were conducted in a three-electrode cell from ALS Co., Ltd, Japan (*ec*-QCM Flow cell kit, used in the stationary mode) under potential scanning condition using a 5 MHz quartz crystal resonator metalized with a gold electrode. The potential was controlled by a potentiostat (Gamry, Interface 1000) and the oscillation frequency was read out with an impedance analyzer (Gamry, *ec*-QCM 10M).

Atomic force microscopy (AFM), electrochemical AFM (ec-AFM), and scanning tunneling microscopy (STM). AFM images were captured with Flex-Axiom “Nanosurf” using Supersharp silicon probe (SSS-NCLR, NANOSENSORSTM) in the dry state, or PointProbe Plus Contact Mode Short Cantilever –Au Coating probe (PPP-NCSTAuD NANOSENSORSTM) for *ec*-AFM on the Electrochemistry Stage ECS 204 in 0.1 M aqueous electrolyte. The potential of the modified GC electrode was stepped versus an Ag/AgCl reference electrode using a Pt wire counter electrode and a potentiostat (Gamry, Interface 1000). STM imaging was carried out with an EasyScan Nanosurf instrument at room temperature using typically 0.050 V bias voltages and 1.000 nA tunneling current (all images were taken in constant current mode). The images are raw data without filtering. The STM tips were cut from Pt/Ir wire (0.25 mm, Schaefer Technologie GmbH, Langen, Germany). The reduced composite-covered HOPG electrode (5*5 mm piece) was glued onto the magnetic support and the surface was electrically connected to the support with silver lacquer painted over the glass edge.

Battery fabrication. A test full-cell was fabricated using a PCo@rGO electrode (0.75 μm, 55 mC cm^{-2}) and a PFc@rGO electrode (0.79 μm, 21 mC cm^{-2}). Both battery materials were binder free and contained 5 wt % rGO. They were deposited on glassy carbon or graphite electrodes and the Swagelok-type cell was measured in an aqueous solution of 1 M $LiClO_4^-$ using Celgard 2325 (thickness 25μm, porosity: 39%) as a separator. All the electrochemical tests were performed at room temperature.

Instrumentation. Sonication was performed in an ultrasonic bath (VWR USC300TH, 80W).

2- PCo@GO self-assembly

The composite material is prepared based on electrostatic interaction between positively charged PCo^+ and negatively charged GO^-, *i.e.,* single layer graphene oxide (GO^-) sheets in aqueous solution (Figure S1a). GO^- shows a negative Zeta (ζ) potential (-36.9 mV), which is related to dissociated GO's carboxylic acid groups. Stepwise addition of aqueous PCo^+ aliquots to an aqueous dispersion of GO^- shifts the ζ-potential toward positive values (Figure S1b). At ζ-potential = ~ 0 ($W(PCo^+)/W(GO^-) = 1$) the positive charges on PCo^+ compensate the negative charges on the poly-anion GO^-, and the colloidal solution becomes unstable and starts to precipitate transitionally. Upon further PCo^+ addition the precipitate dissolves again and the ζ-potential continues in a sigmoidal fashion into the positive range reaching a constant value (+35 mV) at a weight ratio polymer: GO = 30 (log ratio = 1.5). Obviously, a multi-layer deposition of PCo^+ on both sides of single GO^- sheets develops (for the optimized electrochemical performance we found an ideal weight ratio of ($W(PCo^+)/W(GO^-)$) = 5 (ζ-potential=29), see later). At such loading, PCo@GO suspensions were stable for at least 8 months (Figure S2).

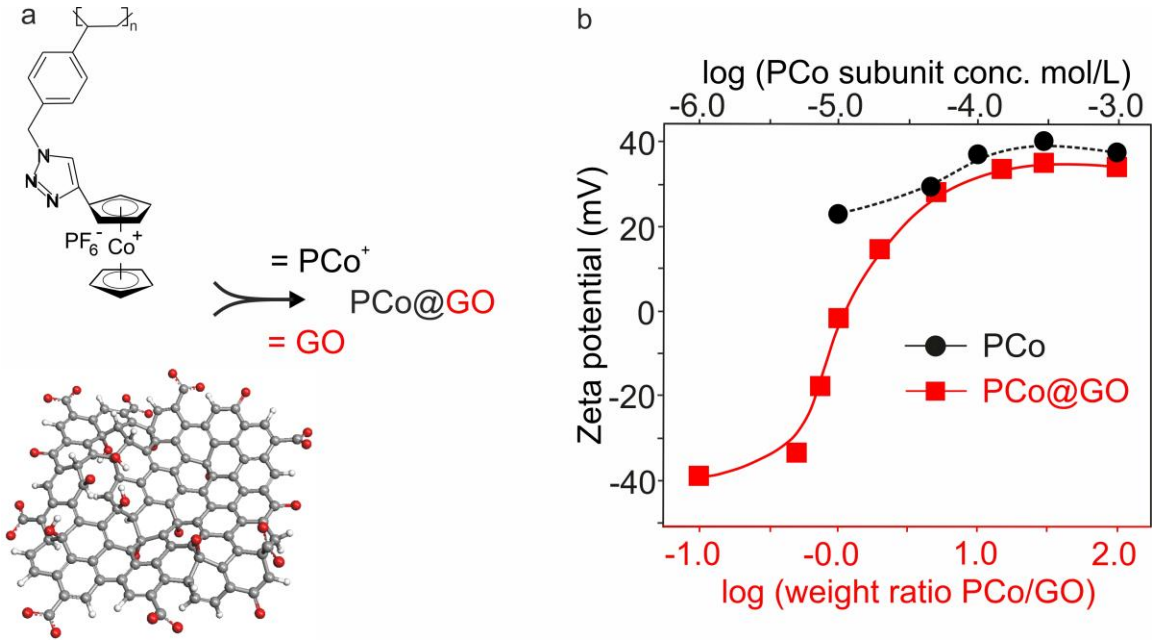

Figure S1. *Self-assembly of PCo^+ and GO^-. a) PCo@GO complex formation between $PCo^+(PF_6^-)$ and GO^-. Red dots in GO^- refer to oxygen atoms carrying a partially negative charge. b) ζ-potential of PCo^+ (black, -●-) and of PCo@GO dispersions (red, -■-) vs. log [PCo^+ subunit conc.] and vs. log [mass ratio PCo/GO] at constant GO^- concentration (0.05 wt %, −40 mV) in H_2O; PCo conc. axis is valid for both curves.*

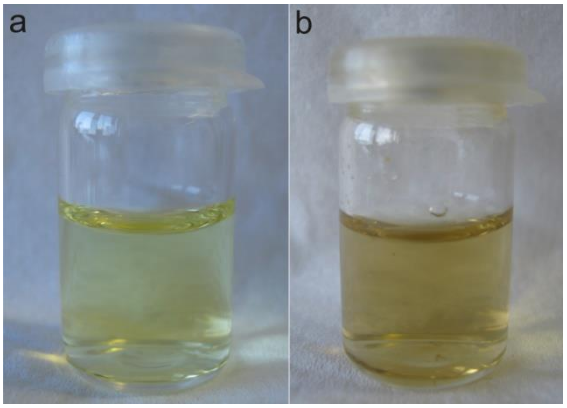

Figure S2. *Colloidal solution stability: $PCo^+(PF_6)^-$ (a) and PCo@GO (b) with a PCo/GO weight ratio of 5 / 1 in H_2O/DMF (14/1) (see preparation in experimental section). Both solutions were stable for at least 8 months.*

3- GO/rGO transformation in PFc@GO composite: redox active catalyzer in the electrolyte solution

It was shown that the functional groups of GO (such as hydroxyl and epoxide functional groups on GO's basal planes and carbonyl and carboxylic groups on the edges) can be reductively removed under acidic conditions (pH = ~5) and by applying a negative potential of −1.5 V (vs SCE).[3] Although, this electrochemical reduction strategy yields highly conductive rGO, the reduction process of thick layers is slow and not efficient. In a recent paper,[4] we have developed a new electrocatalytic method for the GO/rGO transformation using methyl viologen dichloride (MV^{++}) as an electrocatalyst dissolved in the electrolyte solution. MV^{++} is reduced in two steps from the dication via the monocation radical to the neutral species in water. Electrocatalysis occurs from the singly and the doubly reduced state of MV^{++}, with a larger cathodic electrocatalytic contribution on the second wave (Figure S3a).

In Figure S3b, the GO/rGO transformation was catalyzed by cobaltocenium (Cp_2Co^+) (as an alternative to MV^{++}). The electrode potential is scanned in water containing 0.1 M $LiClO_4$/4 × 10^{-3} M Cp_2Co^+ for 5 consecutive scans (0 → 0.8 → -1.25 → 0 V). In the first scan (red line), a weak quasi-reversible wave related to the ferrocene/ferrocenium couple is observed (eq. S2). In the negative potential range, the Cp_2Co^+ wave is recorded. A plateau current, which is typical for electrocatalytic situations can be identified on Cp_2Co^+ reduction wave. The second scan differs largely from the first one, but it is very similar to scan numbers 3 to 5. The electrocatalytic waves are interpreted by the sequence of eq. S1 and S3.

$Cp_2Co^+ + e^- \rightarrow Cp_2Co$	$E^0_1 = -1.2$ V	eq. S1
$PFc^+ + e^- \rightarrow PFc$	$E^0_2 = 0.27$ V	eq. S2
$Cp_2Co + GO^-$ site $\rightarrow$ rGO−site $+ Cp_2Co^+ + H_2O$		eq. S3

$-(CHX)-(CHX)- + 2e- \rightarrow -(CH)=(CH)- + 2X^-$ sp^2 regeneration by reductive elimination

eq. S4

The ultimate reductive elimination (eq. 4) leads to mass loss from the composite (2 X^-, with X^- = any reasonable leaving group, e.g., OH^-, CH_3COO^-) and regenerates sp^2 centers in the graphitic layer (increased electronic conductivity). The enhanced conductivity manifests itself by the approximately five fold current response of the ferrocenium/ferrocene couple for scan number 2 and larger. According to the growing ferrocene response, the reduction of the GO is almost completed after only one cycle.

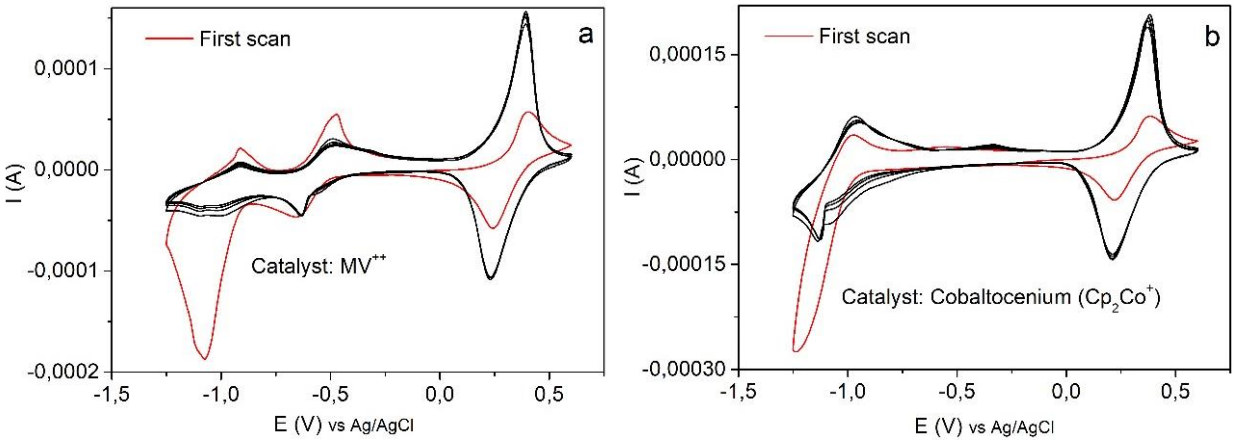

Figure S3. *Repetitive CVs of (PFc@GO)@GC corresponding to ~2 × 10^{-7} mol subunits cm^{-2} in 0.5 M $LiClO_4/H_2O$ + (a) 4 × 10^{-3} M $MV^{++}(2Br^-)$ (electrocatalyst) or + (b) 4 × 10^{-3} M $Cp_2Co^+(PF_6^-)$ (electrocatalyst), at v = 20 mV s^{-1}. First scan (red: -0.2 → 0.6 → -0.2 V): small PFc response at positive potentials, 1st scan continuation (red, -0.2 → −1.2) $MV^{++} \rightarrow MV^{\bullet+}$ and $MV^{\bullet+} \rightarrow MV^0$ (left) or $Cp_2Co^+ \rightarrow Cp_2Co$ (right) reduction + electrocatalysis (GO → rGO transformation); 2nd and later scans (black). The peaks at the negative potentials reprenset the shuttles used to reduced GO and the peaks at postive potentials show the redox reaction of PFc increasing by continuation of scans attribued to the higher conductivity of the electrode upon GO/rGO transformation.*

4. GO/rGO transformation in PCo@GO composite: self-catalysis

The stable colloidal solution was applied to a macroscopic current collector (CC (GC or carbon plate)) by stepwise drop casting/solvent evaporation to yield (PCo@GO)@CC. In order to switch on the electronic conductivity in the nanoscopic current collector, GO needs transformation into rGO.[5] In case of PFc@GO, we used earlier dimethyl viologen ($E^o(Vio^{++}/ Vio^{+\cdot}$ ~ -0.5V, E^o ($Vio^{+\cdot}$ /Vio^o) ~ -1.0V) as an electrocatalyst in the aqueous electrolyte to promote the reduction of GO in the battery material.[4] As shown in Figure S3b, the reduction potential of monomeric $CoCp_2^+$ is poised in the range of the second viologen reduction potential and accordingly it is able to electrocatalysis the GO/rGO transformation in the ferrocene composite. We were therefore confident that the $Cocp_2$ subunit in PCo@GO@CC will also act as an electrocatalyst (Figure S4a). Scanning the potential of a PCo^+@rGO@GC modified electrode repetitively between -0.4 to -1.2 V reveals a redox wave interpreted as eq. S4.

$$PCo^+@rGO + e^- \leftrightarrow PCo^0@rGO \qquad \text{eq. S4}$$

$$PCo^0@GO \rightarrow PCo^+@rGO + H_2O \qquad \text{eq. S5}$$

The additional cathodic current decaying in the first four cycles is typical for the simultaneous and irreversible electrocatalytic GO/rGO transition (eq. S5). During this period and parallel with the disappearance of the catalytic current contribution, the cobaltocenium response becomes more reversible, obviously, because the electronic conductivity of the nanoscale current collector increases (narrowing peak separation in Figure S4a). The eQCM frequency responses of (PCo@GO)@Au during the first 10 consecutive CV cycles is in agreement with this interpretation (Figure S4b, see Figure S5 for more details). An irreversible weight loss during the initial 5 scans and a reversible frequency response after this period is observed. The GO/rGO transition is related to the initial mass loss Δm_1 = 5.13 µg cm^{-2} (290 Hz). However, it is overlaid by a complicated ion exchange reaction (PCo's anion (PF_6^-) exchanges to Cl^-(partially) with GO's surface bound

negative functional groups during complexation and Cl^- of the supporting electrolyte moves during charge-discharge cycling). Thus, an accurate calculation of the weight loss is not possible. However, our previous report on PFc@GO showed ~47 wt% loss of oxygen functional groups from GO in the first few cycles.[4]

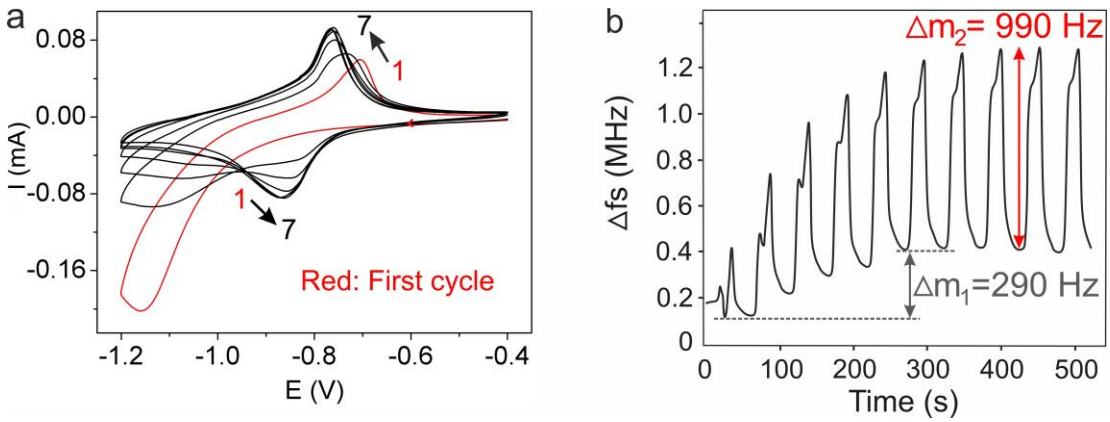

Figure S4. *Electrochemical transformation of PCo@GO to PCo@rGO. a) electrocatalytic PCo@GO → PCo@rGO transformation, repetitive CVs of (PCo@GO)@GC (mass density 86 µg cm^{-2}, PCo_{mol} subunit/cm^{-2} = 1.38×10^{-7}, in 0.5 M / KCl at v = 50 mV s^{-1}); 1st scan: eq. 1) and 2), 7th scan: only eq 1; b) eQCM frequency responses for 9 consecutive CV scans (see Figure S5a for corresponding CVs); mass density loss: (Δm_1, black) = 5.13 µg cm^{-2} (290 Hz) due to GO/rGO transformation from extrapolated irreversible change (dotted magenta curve), attribute to 47% GO weight loss;[4] reversible mass density changes: (Δm_2, red) = 17.5 µg cm^{-2} (990 Hz) due to the Cl^-/H_2O (de)insertion upon PCo^+/PCo^0 transition.*

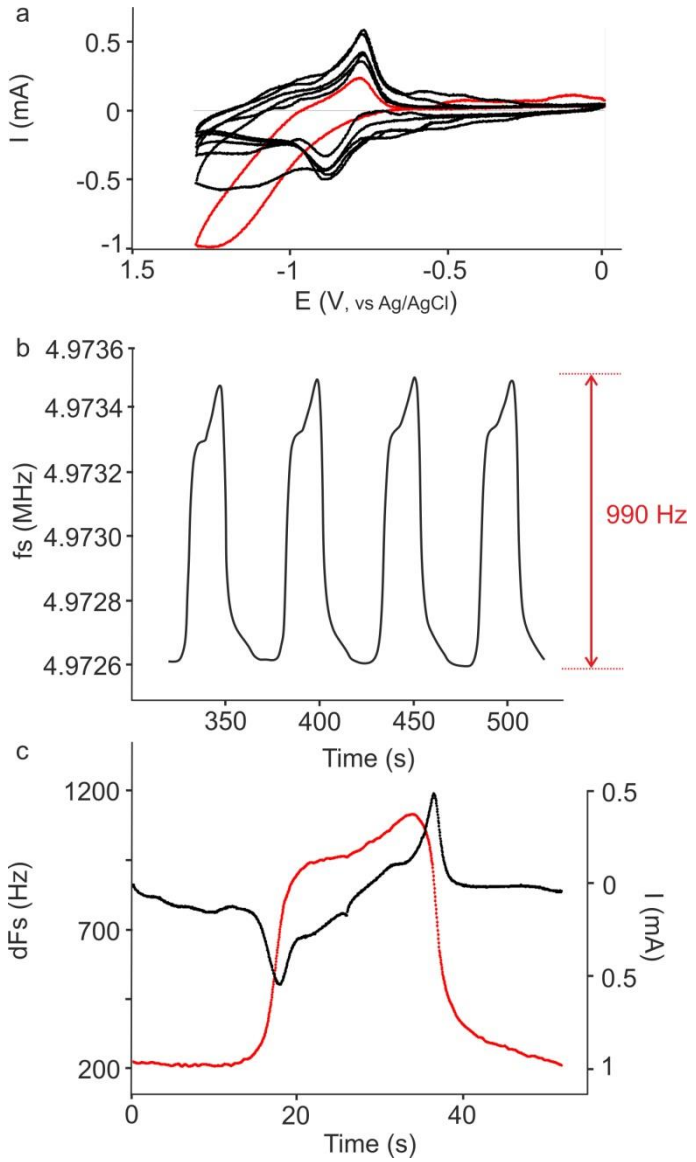

Figure S5. *Electrocatalytic PCo@GO → PCo@rGO transformation (PCo/rGO=5). (a) Repetitive CVs of (PCo@GO)@Au (polymer subunit density 141.5µg cm^{-2} in 0.5M/KCl at v = 50 mV s^{-1}); corresponding to Figure S4b. (b) eQCM frequency responses for 5 consecutive CV scans after GO/rGO transformation (extracted from Figure S4b); Δf = 990 Hz due to the Cl$^-$/H$_2$O (de)insertion from/into PCo$^+$/PCo° transition (see details of no. water in Figure S10 and Table S1); (c) Simultaneous mass (red, eQCM, from b) and current (black, from CV, a) from one experiments.*

The electrochemical AFM (*ec*-AFM) method was also used to determine height change upon the GO/rGO transformation (Figure S6). It was observed that electrochemical removal of oxygen

functional groups in KCl solution results in 4.8% height decrease *i.e.*, 0.961 → 0.915 µm. Moreover, AFM analysis in the x-y plane revealed small changes in the diameter and connectivity of the pores, however, the typical topographic structures have not dramatically changed.

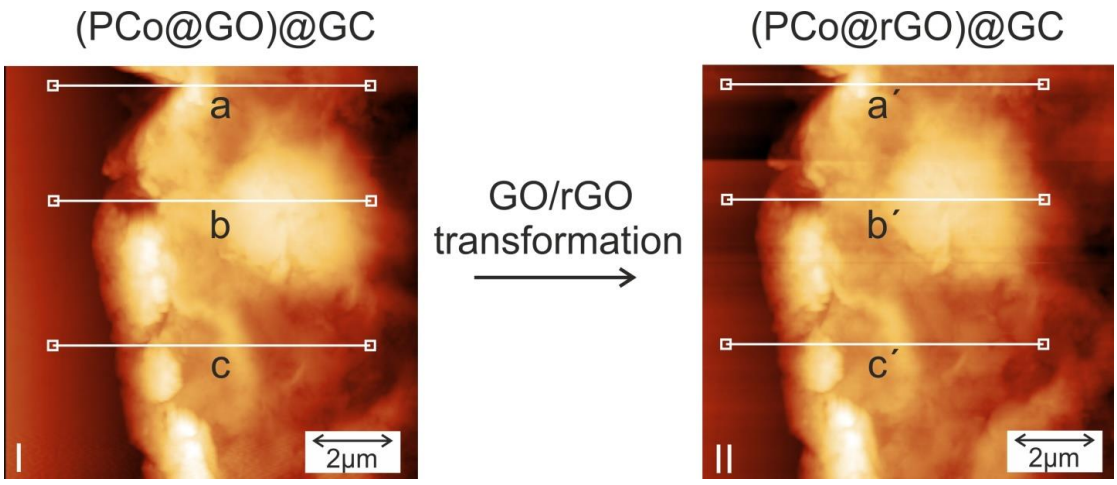

Figure S6. *GO/rGO transformation, AFM. Electrochemical AFM images of (PCo@GO)@GC (I) and (PCo@rGO)@GC (II) captured from the same region before (I) and after (II) GO / rGO transformation. Both analyses measured under a constant potential = 0 V in 0.1 M KCl/H_2O. Arbitrarily selected cross sections at the same place indicate a decrease of height between the GC plane (right) and the composite top (left) from 935, 968 and 979 (a – c) to 913, 916 and 916 nm (a´ – c´), due to the GO / rGO transition. The reduction results to average height change from 961 to 915 nm, which translates to 4.8 % height decrease upon reduction.*

5. Electrochemical characterization of PCo@rGO

The influence of the percentage of conductive additive on energy storage performance is evaluated by measuring the coulombic efficiency of composites using various ratios of PCo/rGO. (Figure S7a). The highest coulombic efficiency (> 99%, calculated f/rom the discharge capacity in a galvanostatic study, Figure S7b) was achieved for a ratio of 9.5/1. Higher and lower ratios of electron storage material to conductive filler diminish the observed charge. Notably, the low coulombic efficiency of the pure polymer (6%) was significantly enhanced by the addition of only ~2 wt % rGO (57%). The beneficial influence of the rGO content becomes more evident from a series of galvanostatic measurements on pure polymer and composite measured at different rates (1–100 A g^{-1}) (Figure S7c). In case of the composite at a fast discharging rate (100 A g^{-1}), the observed capacity drops only by 20%, while the pure polymer response drops to ~0 % already at 50 A g^{-1}. Remarkably, this mechanism allowed preparation of thick layers up to 1.24 C cm^{-2}, a significantly higher value than previously reported metallocene electrodes. The pure polymer is not thickness scalable beyond 0.2 µm. It clearly shows the importance of the electron/ion percolation system introduced by the reduced graphene oxide, which is covered by a ca. 10 nm thick layer of the cobaltocenium polymer.

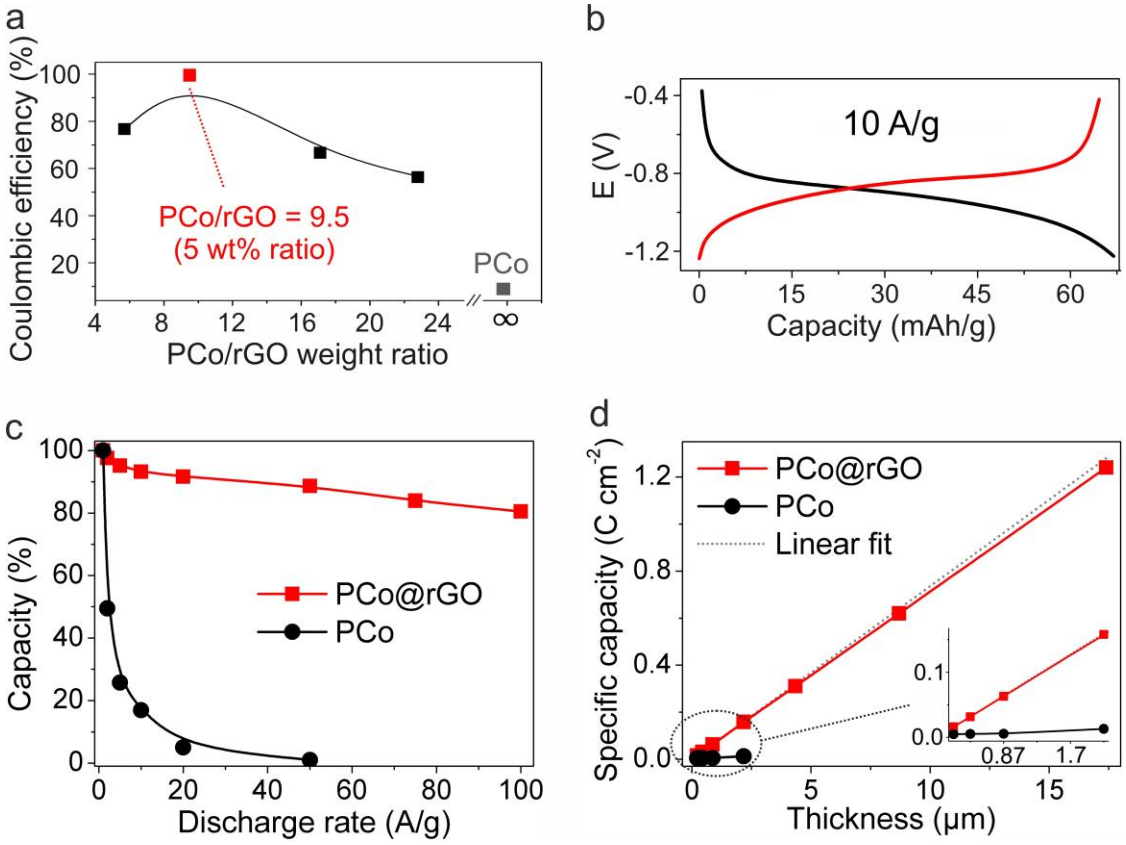

Figure S7. *Electrochemical characterization of PCo@rGO. a) PCo/rGO ratio optimization. Anodic charge from (PCo@rGO)@GC for varying PCo/rGO ratios at constant PCo surface concentration: 93.9 μg/cm^2, 1.8×10^{-7} mol cm^{-2}, from discharge capacity of obtained from galvanostatic curves (b) as a function of PCo/rGO weight ratio; electrolyte: 0.5M KCl/H$_2$O. c) percentage obs. capacity* vs. *discharge rate of composite (–■–, red) and polymer (–●–, black) films in 0.5 M KCl/H$_2$O with max. obs. capacity: 1.9 mC cm^{-2}, from galvanostatic measurements. d) Areal capacity as a function of thicknesses of composite on GC with PFc/rGO ratio of 10.4 (−■−, red) and 0, i.e., pure polymer (−●− black), obtained from anodic waves in CV, at v = 2−20 mV s^{-1}.*

6- Structure and morphology analyses of PCo@GO and PFc@GO composites

PCo@GO: For AFM structural analysis, the PCo@GO composite was drop casted onto glassy carbon (GC) (Figure S8c, S8d) and was compared with the topology of its pure components: PCo@GC (Figure S8a) and GO@GC (Figure S8b). The pure polymer shows a relatively smooth but granular surface (granules extending over 50-100 nm (AFM tip resolution limited)) with a few pores (ca. 100 nm deep). The pure GO displays typical stacked, folded veils with soft edges extending over 50 to >1000 nm and a prominent tendency for 100 nm deep pore formation (lateral size 100-400 nm). (PCo@GO)@GC with only 5 wt% GO adopts mainly the structural features of pure GO, but shows deeper pores (0.1-2 µm) and sharper edges (Figure S8c). Zoom-in image (Figure S8d) reveals a few PCo polymer strands on top of GO and extending into the pores of GO (d1 and d2), but these do not account for 95% of the PCo^+ material. In order to find/localize the polymer chains, we switched to STM and replaced - for analytical purpose - GO by edge oxidized, semiconducting carbon nanotubes (6,5-CNTs). These CNTs exhibit the same efficient PCo^+ wrapping but they offer much higher resolution down to the sub-nanometer range known for other electroactive polymers on CNTs.[6] Figures S8e and Figure S8g show tight helical PCo^+ wrapping in a mono- or multi-layer on CNTs, respectively. Single polymer chains in different layers can be identified. Their experimental diameters fit the expected 2.2 nm (Figure S8f) predicted from semiempirical PM6 modeling (Figure S8h and S8i). The same study on PFc@CNT (Figure S9) reveals again helical wrapping in mono- and multilayers on CNTs. The increased experimental and theoretical polymer diameter for PCo^+ (2.2 nm) as compared to PFc^+ (1.1 nm) reflects the additional benzyl triazole subunit in PCo^+. In conclusion, PFc^+ and PCo^+ undergo self-assembly with CNT^- and GO^-. At least on CNT, but most probably as well on GO, the polymer layer consists of tightly packed parallel polymer chains. Depending on the polymer/GO weight ratio used during their preparation, partial coverage, complete monolayers or multilayers of polymer develops. The material exhibits a nanoscopic percolation system mainly generated by the GO structure for ions and for electrons (upon the intended GO → rGO transformation (see later)). The tight polymer

layer in close contact with rGO reduces electron propagation by a hopping mechanism to values <10 nm even when using polymer/GO weight ratios > 20. Such structural and functional conditions will of course only persist if the GO/rGO transition proceeds smoothly.

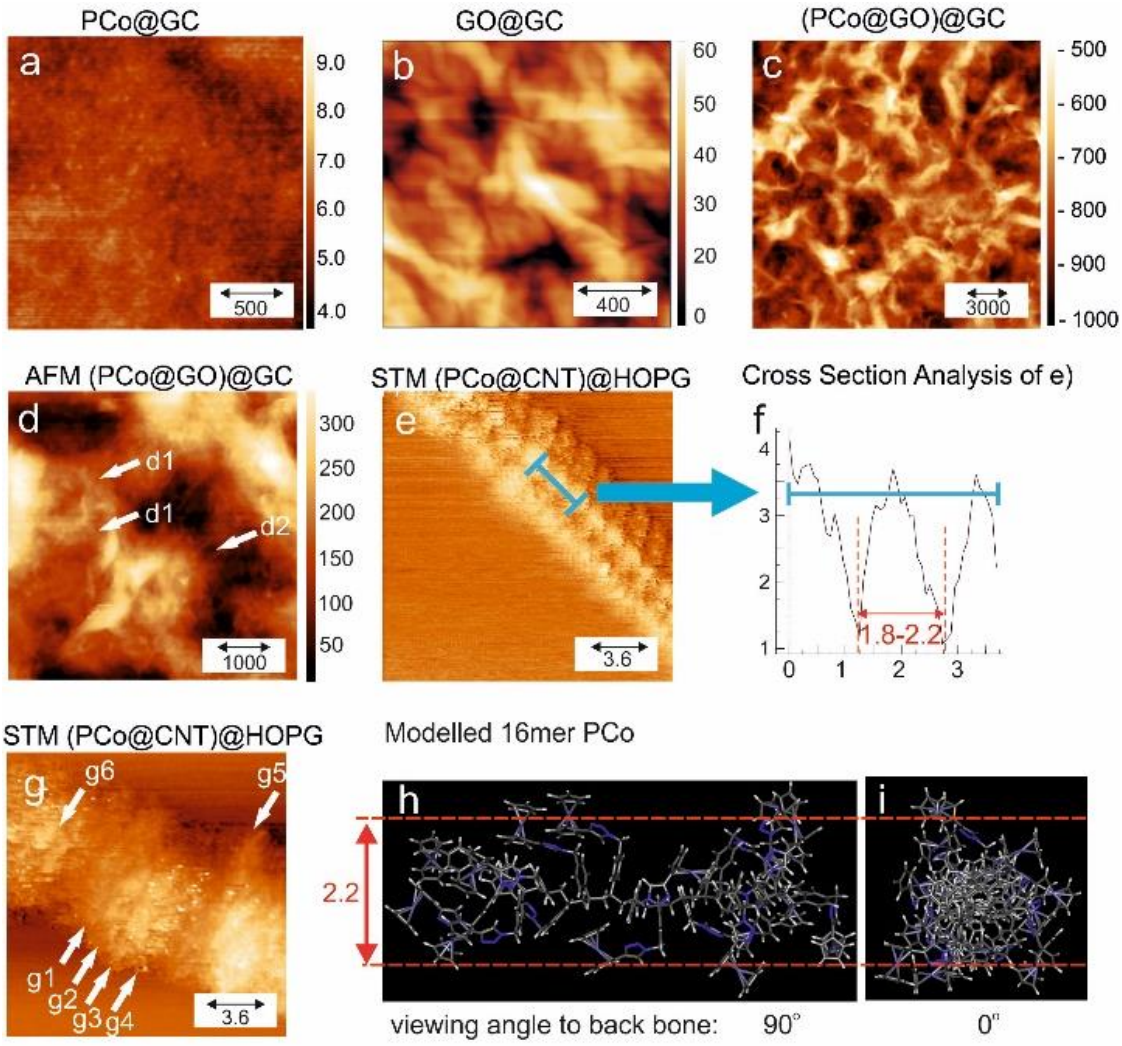

Figure S8. *Structural analysis. a) AFM PCo^{+}@GC (11 µg cm^{-2}; b) AFM GO^{-}@GC (12 µg cm^{-2}); c) AFM (PCo@GO)@GC, 14 µg cm^{-2}; d) (PCo@GO)@GC (zoom-in), 14 µg cm^{-2}, d1: polymer strands on top of GO, d2: polymer strands in GO tunnel. e) STM (PCo@CNT)@HOPG with helical single PCo chains wrapping 1(or 2) CNTs and corresponding chain diameter analysis in f); g) STM helical CNT wrapping by PCo in multi layers g5-g6, displaying single chain resolution mainly in lower layers (g1-g4); gas phase PM6 semiempirical modeling of 18mer PCo. All numbers without units in nm.*

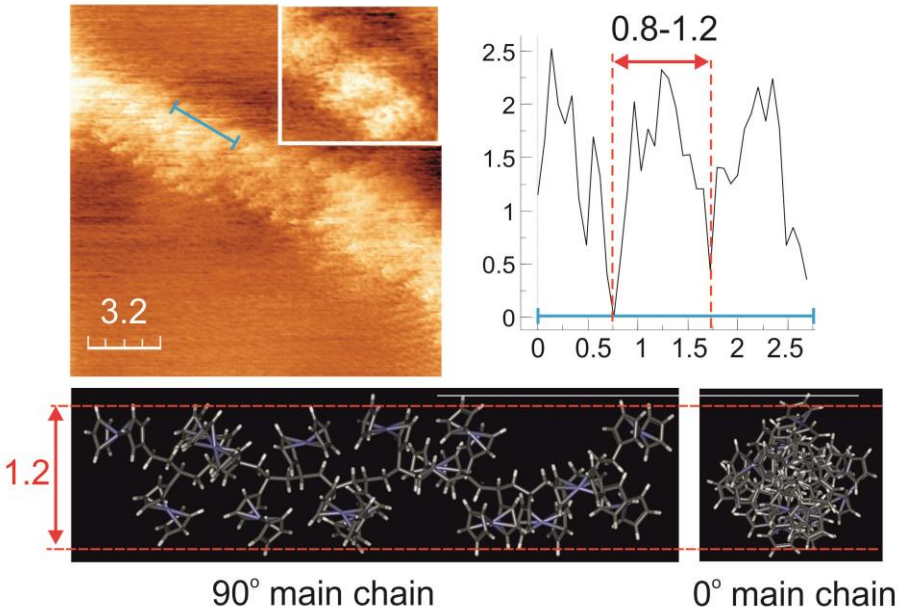

Figure S9. *PVFc@CNT and PM6 modeling of PVFc in the gas phase. STM of PVFc wrapping a CNT in mono- and multilayer fashion with cross-section analysis and PM6 model of a 16-mer PVFc chain. A diameter of 0.8-1.2 nm was experimentally found for the PVFc (as compared to 1.8-2.2 nm for PCo@CNT, Figure S8). The diameters from modeling are ca. 1.2 nm for PVFc and 2.2 nm for PCo (Figure S8).*

7- Supporting electrolyte optimization

Cation optimization:

The frequency changes (Hz, translated to µg using Sauerbrey equation, constant: 56.6 Hz μg^{-1} cm^2), and electrochemical responses in four aqueous based electrolytes with different cations (Li^+ , K^+ , NH_4^+ , $(Bu)_4N^+$) (Figure S10a-d) and similar anion (Cl^-) have been examined (Table S1). It was observed that changing the cation of supporting salts did not have big influence on the magnitude of the frequency changes (Table S1) and neither on the redox potentials of PCO@rGO. This shows that the weight changes of the composites during charging-discharging is counterbalanced mainly by anion movement

Anion optimization:

Five anions of different size and hydrophilicity were chosen: Cl^-, I^-, BF_4^-, ClO_4^- and PO_4^- (Figure S10a, S10e-h). It was observed that anion variation considerably alters the mass changes (Table S1) and CV response (j). This demonstrates that the breathing ion is an anion. Compared to Cl^-, the cathodic waves of polymer ($PCo^+ \rightarrow PCo$) in the case of other anions are broader and shifted to more negative values. This can be explained by the higher hydrophobicity of other anions resulting in ion pairing with cobaltocenium (i) and/or by their significantly bigger radii (Table 2, main text), which slows down diffusion/migration throughout the substrate's pores (ii).

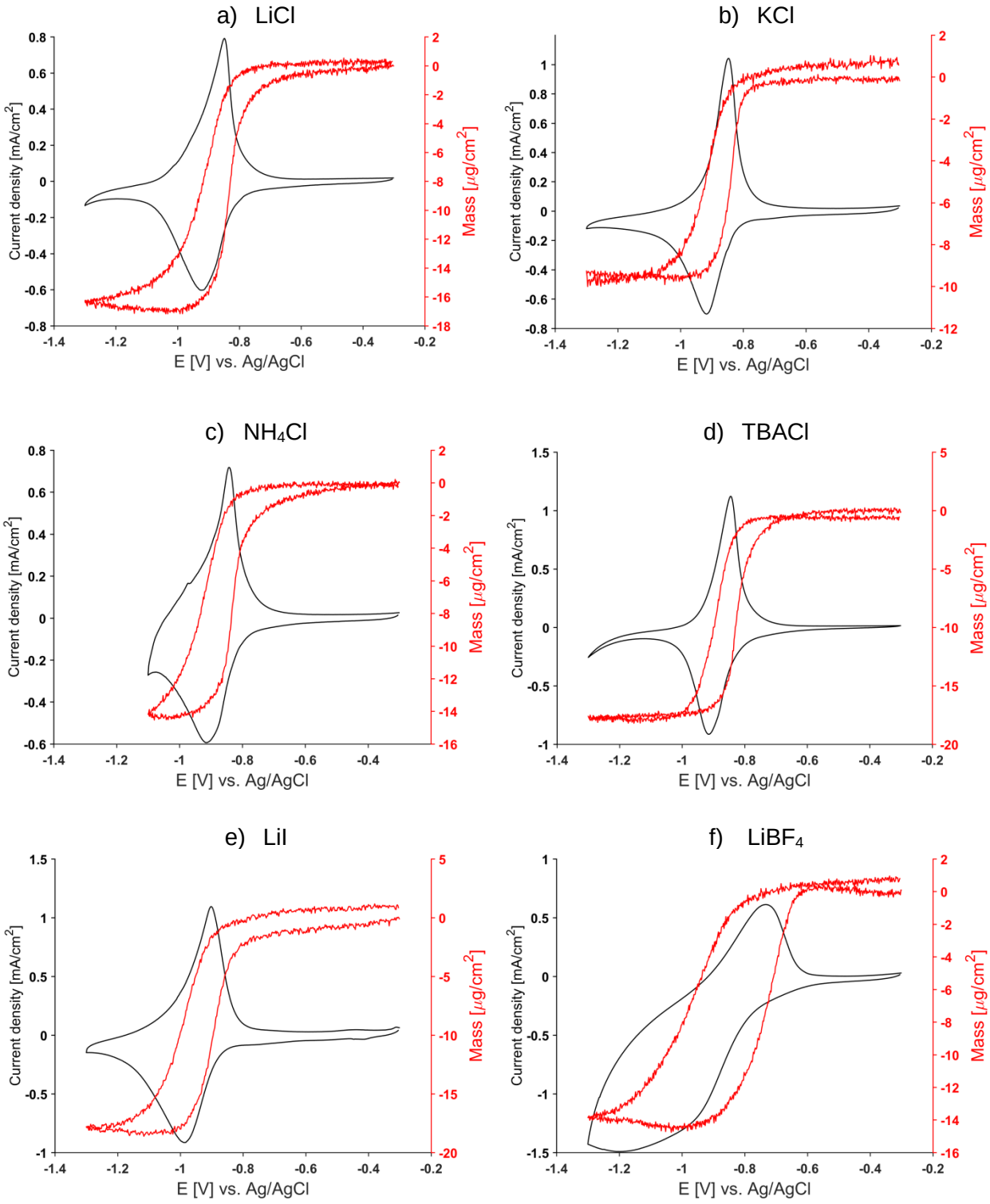
a) LiCl
b) KCl
c) NH4Cl
d) TBACl
e) LiI
f) LiBF4
Current density [mA/cm2]
Mass [μg/cm2]
E [V] vs. Ag/AgCl

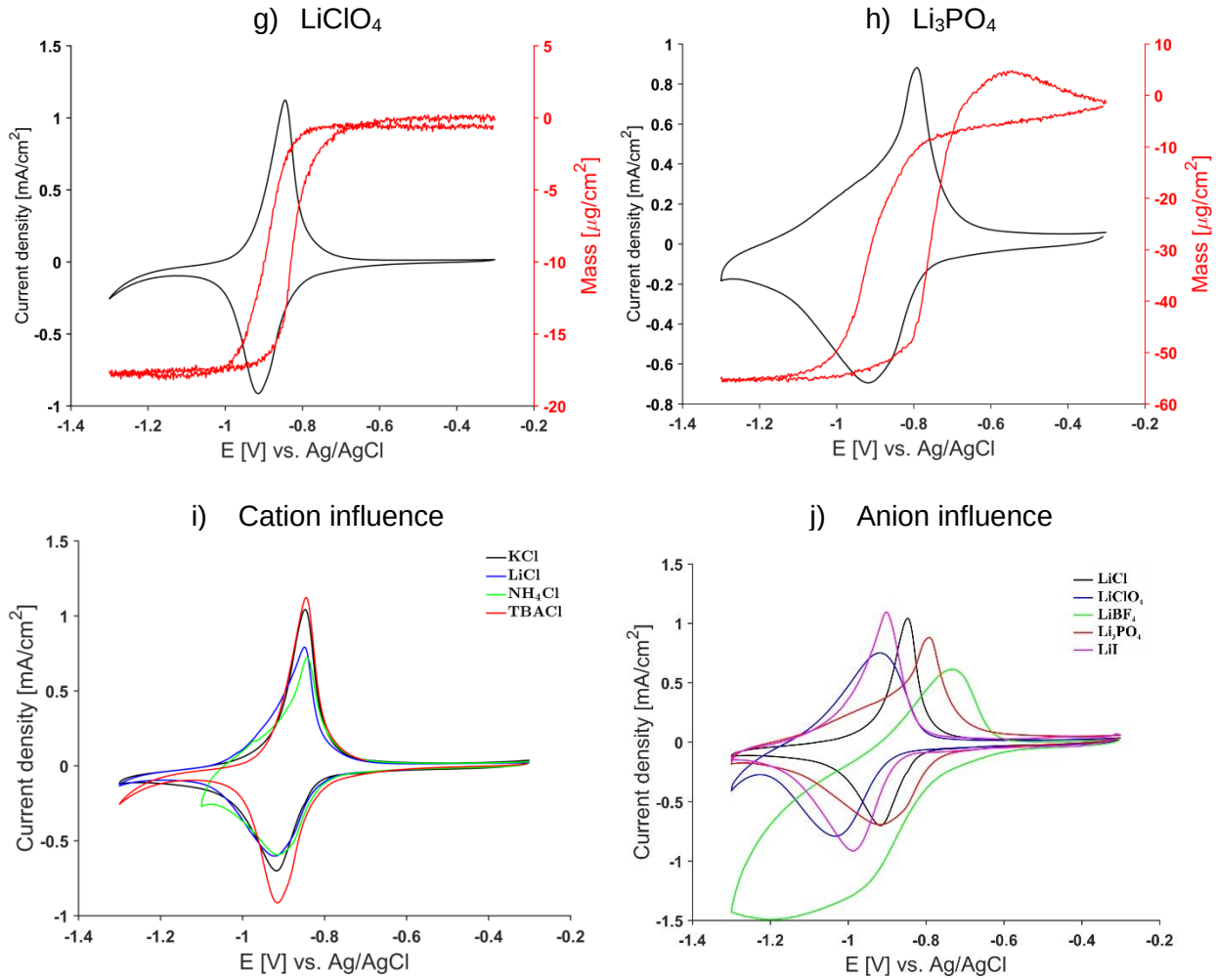

Figure S10. CV/QCM analyses of PCO@rGO using different electrolyte salts.

		Q [mC/cm^2][a]	M [ug/cm^2][b]	no. H_2O[c]	E_{red} [mV][d]	E_{ox} [mV][d]	Δ E [mV]
	cation influence using constant anion Cl^-						
a	LiCl	9,29	10,41	4,04	-920	-830	90
b	KCl	12,4	9,69	2,2	-920	-843	77
c	NH_4Cl	10,05	14,34	5,68	-914	-842	72
d	TBACl	10,41	17,35	6,96	-916	-842	74
	anion influence using different cations						
e	$LiClO_4$	12,76	13,27	1.13	-1036	-922	114
f	$LiBF_4$	16,79	15,15	0,01	-1.186	-731	366
g	$Li_3PO_4^*$	19,39	53,16	9,42	-920	-790	130
h	LI	14,34	19,29	0,18	-992	-901	91

Table S1. CV/QCM data extracted from Fig. S6a-j)

a: charge, calculated from integration of the anodic PCo composite wave.

b: mass, obtained from frequency change of modified quartz crystal during charging-discharging. The frequency is translated to mass using the Sauerbrey equation.
c: calculated from eQCM analyses (Figure S10)
d: potential *vs.* Ag/AgCl
*: pH not adjusted

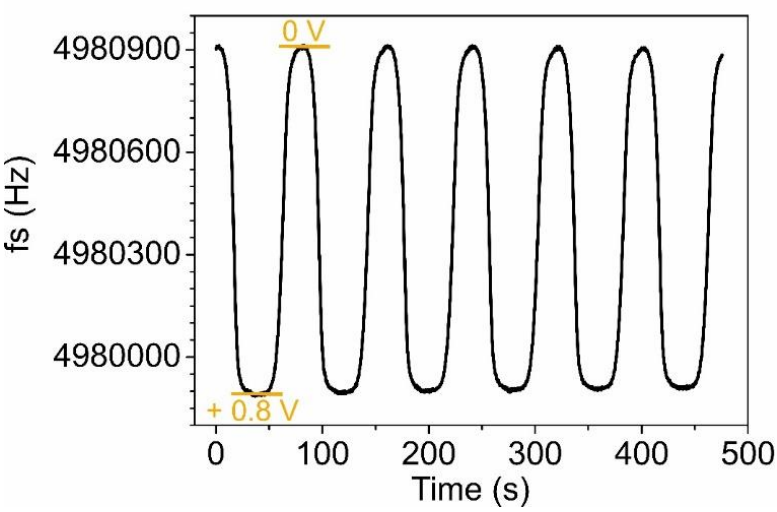

Figure S11. *eQCM analysis of PFc@rGO in 0.1 M $LiClO_4$.*

8- Height oscillation from chloride breathing: electrochemical AFM

a: Electrolyte: 0.1 M KCl/aq.

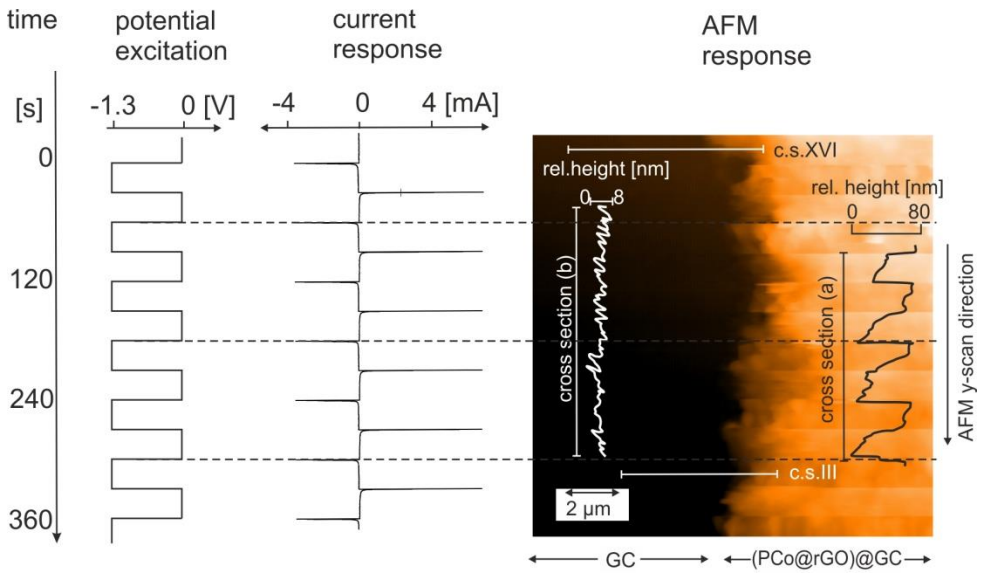

Figure S12 Electrochemical redox switching of (PCo@rGO)@GC during AFM image acquisition. Electrochemistry: electrolyte: 0.1 M KCl/H_2O,excitation: square wave potential: 0 → - 1.3 → 0 → …. (13 steps with 30 s step time), current response (chronoamperometric): anodic (positive current (right)) and cathodic spikes. AFM image: (PCo@rGO)@GC (PVFc@rGO with weight ratio PCo^{x+}/GO^{m-} = 5) on 0.07 cm^2 GC; left part of image: GC (PCo@rGO scratched away), AFM scan direction downwards, total AFM acquisition time: 400s, 13 potential steps during AFM acquisition correlate with 13 stripes (dark/light) in the composite covered region but not in the scratched region (vertical cross section a and b in y-direction): average height increase upon oxidation: 80 nm; averaged height change: 7.64% (Table S2).

Table S2 *The calculated difference between the averaged heights of oxidized and reduced states is 80 nm, i.e., 7.64 % with respect to PCo@rGO in the oxidized state (observed capacity: 75 mC cm^{-2}).*

	Oxidized:	Reduced
	1.04	0.987
	1.01	0.893
	1.078	0.983
	1.114	1.007
	1.084	0.992
	0.970	0.916
	1.065	1.017
Sum:	7.361	6.795
Average:	**1.051**	**0.971**

b: Electrolyte: 0.1 M Na_3PO_4/aq.

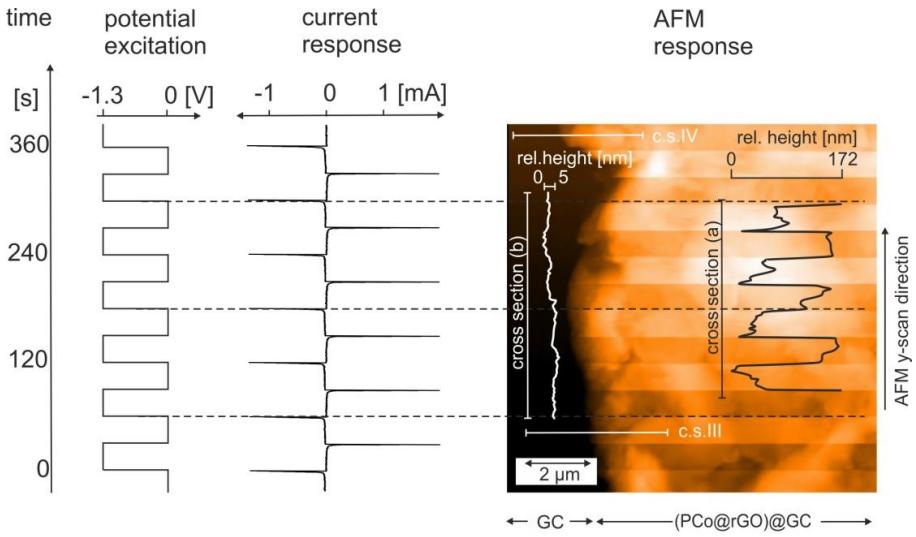

Figure S13. *Electrochemical redox switching of (PCo@rGO)@GC during AFM image acquisition. Electrochemistry: electrolyte: 0.1 M Na_3PO_4/H_2O, excitation: square wave potential: 0 → - 1.3 → 0 → …. (13 steps with 30 s step time), current response (chronoamperometric): anodic (positive current (right)) and cathodic spikes. AFM image: (PCo@rGO)@GC (PVFc@rGO with weight ratio PCo^{x+}/GO^{m-} = 5) on 0.07 cm^2 GC; left part of image: GC (PCo@rGO scratched away), AFM scan direction upwards, total AFM acquisition time: 400s, 13 potential steps during AFM acquisition correlate with 13 stripes (dark/light) in the composite covered region but not in the scratched region*

(vertical cross section a and b in y-direction): average height increase upon oxidation: 172 nm; averaged height change: 13.43% (see Table S3).

Table S3. The calculated difference between the averaged heights of oxidized and reduced states is 172 nm, *i.e.,* 13.43 % with respect to PCo@rGO in the oxidized state (observed capacity: 61 mC cm^{-2}); electrolyte: 0.1 M Na_3PO_4/aq.

	Oxidized:	Reduced
	1.278	1.04
	1.019	0.865
	1.195	1.113
	1.316	1.135
	1.475	1.236
	1.331	1.133
	1.349	1.237
Sum:	8.963	7.759
Average:	**1.28**	**1.108**

c: other salts: KI, $NaBF_4$, and $LiClO_4$

Similar measurements as in a and b were performed to evaluate the height change using an aqueous solution of 0.1 M KI, $NaBF_4$ and $LiClO_4$ and the results are reported and discussed in the main text (Table 2).

9- reciprocal ion breathing

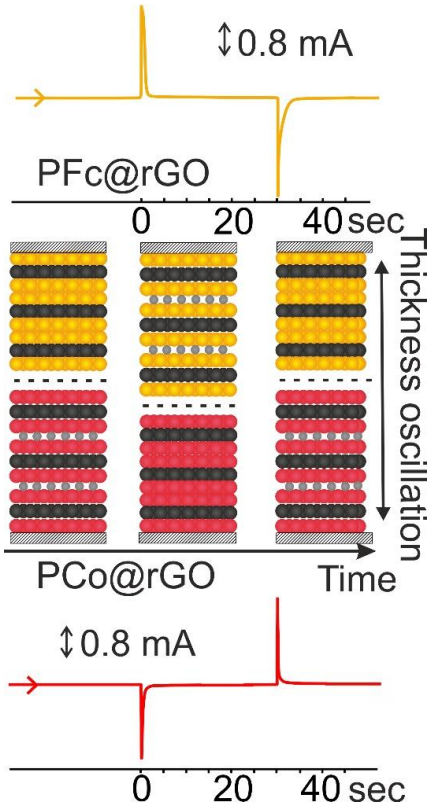

Figure S14. *Reciprocal height change during charging and discharging of the test cell. Orange: PFc, red: PCo, black: rGO, gray: ClO_4^-, dashed lines: separator. Amperometry of PFc@rGO (orange, cut off voltage 0.7 – 0) and PCo@rGO (red, cut off voltage -1.3 – -0.4), electrolyte: 0.1 M $LiClO_4$/aq. A common counter anion (ClO_4^-) is penetrating into the cathode and anode during charging-discharging (a rocking chair system), which allows a reciprocal volume changes and thus prohibit pressure development in the cell. The stress-free volume changes in this metallocene – rGO battery design, make this battery safer (no pressure development), faster (composite layers open up for ion (de)penetration) and more stable over cycling (in contrast to lithium-ion battery, the flexible composite structure does not crack upon ion intercalation).*

10- Amperometry of PCo@rGO in $LiClO_4/H_2O$

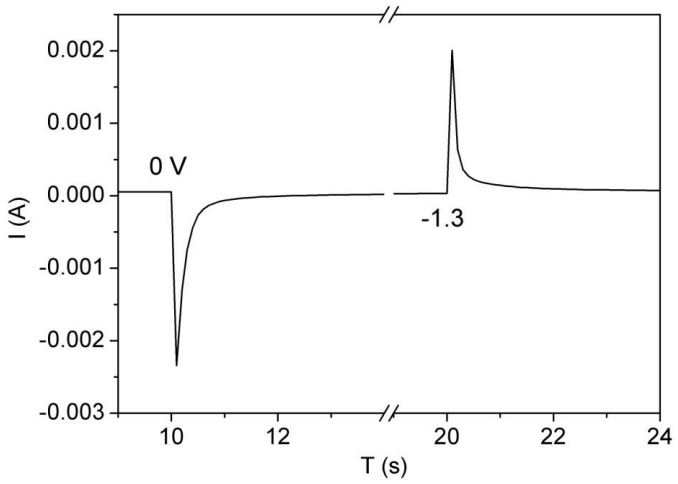

Figure S15. Amperometry of PCo@rGO composite films on GC in 1 M $LiClO_4/H_2O$; PCo_{mol} subunit/cm^{-2} = 7. 6 ×10^{-5} mol/cm^2; potential step: 0 and -1.3 V (*vs.* Ag/AgCl).

References

[1] M. Gallei, R. Klein, M. Rehahn, *Macromolecules* **2010**, *43*, 1844-1854.
[2] A. Rapakousiou, Y. Wang, J. Ruiz, D. Astruc, *J. Inorg. Organomet. Polym. Mater.* **2014**, *24*, 107-113.
[3] H.-L. Guo, X.-F. Wang, Q.-Y. Qian, F.-B. Wang, X.-H. Xia, *ACS Nano* **2009**, *3*, 2653-2659.
[4] S. M. Beladi-Mousavi, S. Sadaf, L. Walder, M. Gallei, C. Rüttiger, S. Eigler, C. E. Halbig, *Adv. Energy Mater.* **2016**, *6*, 1600108.
[5] B. Khezri, S. M. Beladi Mousavi, L. Krejčová, Z. Heger, Z. Sofer, M. Pumera, *Adv. Funct. Mater.*, *29*, 1806696.
[6] L. Cao, S. Sadaf, S. M. Beladi-Mousavi, L. Walder, *Eur. Polym. J.* **2013**, *49*, 1923-1934.